Disease Models & Mechanisms 5, 948-955 (2012) doi:10.1242/dmm.009274

Reduced bone morphogenetic protein receptor type 1A signaling in neural-crest-derived cells causes facial dysmorphism

Hiromitsu Saito[1], Ken-ichi Yamamura[2] and Noboru Suzuki[1,*]

SUMMARY

Bone morphogenetic protein (BMP) receptor type 1A (*BMPR1A*) mutations are associated with facial dysmorphism, which is one of the main clinical signs in both juvenile polyposis and chromosome 10q23 deletion syndromes. Craniofacial development requires reciprocal epithelial/neural crest (NC)-derived mesenchymal interactions mediated by signaling factors, such as BMP, in both cell populations. To address the role of mesenchymal BMP signaling in craniofacial development, we generated a conditional knockdown mouse by expressing the dominant-negative Bmpr1a in NC-derived cells expressing the myelin protein zero (*Mpz*)-*Cre* transgene. At birth, 100% of the conditional mutant mice had wide-open anterior fontanelles, and 80% of them died because of cleft face and cleft palate soon after birth. The other 20% survived and developed short faces, hypertelorism and calvarial foramina. Analysis of the NC-derived craniofacial mesenchyme of mutant embryos revealed an activation of the P53 apoptosis pathway, downregulation of both *c-Myc* and *Bcl-XL*, a normal growth rate but an incomplete expansion of mesenchymal cells. These findings provide genetic evidence indicating that optimal Bmpr1a-mediated signaling is essential for NC-derived mesenchymal cell survival in both normal nasal and frontal bone development and suggest that our model is useful for studying some aspects of the molecular etiology of human craniofacial dysmorphism.

INTRODUCTION

Bone morphogenetic proteins (BMPs) function via conserved type 1 and type 2 transmembrane receptors to regulate a range of biological processes, including cell proliferation, apoptosis, differentiation and cell shape, in a highly context-dependent manner (Massagué, 2000; Chen et al., 2004; Aubin et al., 2004; Kishigami and Mishina, 2005; Eblaghie et al., 2006).

Humans with germ line BMP receptor 1A (*BMPR1A*) mutations that produce truncated receptors suffer from juvenile polyposis syndrome and facial defects (OMIM ID: 174900) (Zhou et al., 2001). Truncated BMPR1A might act via dominant-negative mechanisms. Furthermore, chromosome 10q23 deletion syndrome (OMIM ID: 612242), which is associated with *BMPR1A* deletion, is marked by facial dysmorphism (Delnatte et al., 2006; Menko et al., 2008).

Vertebrate facial development starts with the emergence of five facial primordia: a frontonasal prominence and the paired maxillary and mandibular processes. These primordia mainly consist of neural crest (NC)-derived mesenchyme covered by epithelium (Chai and Maxson, 2006). Whereas the processes grow out in conjunction with regulated mesenchymal cell proliferation and apoptosis (Minkoff, 1980; Beverdam et al., 2001), the paired lateral and medial nasal processes bilaterally bulge at the frontonasal prominence. Then, two fusions occur: one in the midline between the right and left medial nasal processes and the other laterally between the maxillary and nasal processes. Cleft face is caused by the former fusion defect and cleft lip by the latter.

Bmpr1a is broadly expressed and its ligands, *Bmp2*, *Bmp4* and *Bmp7*, are expressed at specific developing nasal regions (Danesh et al., 2009; Furuta and Hogan, 1998; Hu and Marcucio, 2009; Panchision et al., 2001). Previously, researchers generated three conditional Bmpr1a knockout mouse lines (Liu et al., 2005; Nomura-Kitabayashi et al., 2009; Stottmann et al., 2004). However, two mice died in the late embryonic stage and the other displayed no recombination in the mesenchymal cells of the nasal processes. To overcome these issues, we have established a new Bmpr1a-mediated signaling knockdown mouse line in NC cells and confirmed that the signal is involved in craniofacial developmental processes.

RESULTS

Expression and effect of dominant-negative Bmpr1a (Y176STOP) mutant in NC cells

The dominant-negative Bmpr1a protein (dnBmpr1a), which lacks the intracellular kinase domain, inhibits the Bmpr1a-mediated signaling pathway in vivo (Suzuki et al., 1994; Maéno et al., 1994). We generated a *Tg(CAG-flox-dnBmpr1a-NLLacZ)1Nobs* mouse line using the construct *pCAG-XstopX-dnBmpr1a-IRES-NLLacZ* (Fig. 1A). The *Tg(CAG-flox-dnBmpr1a-NLLacZ)1Nobs*$^{tg/tg}$ mice were normal. To generate *Tg(CAG-flox-dnBmpr1a-NLLacZ)1Nobs*$^{tg/+}$*;Tg(Mpz-cre)94Imeg*$^{tg/+}$ mice (hereafter referred to as double-tg) expressing dnBmpr1a in NC cells, we crossed *Tg(CAG-flox-dnBmpr1a-NLLacZ)1Nobs*$^{tg/tg}$ mice with *Tg(Mpz-cre)94Imeg*$^{tg/+}$ mice (Yamauchi et al., 1999). Controls throughout the study were single transgenic littermates without *Cre* transgene.

[1]Department of Animal Genomics, Functional Genomics Institute, Mie University Life Science Research Center, 2-174 Edobashi, Tsu, Mie 514-8507, Japan
[2]Department of Developmental Genetics, Institute of Molecular Embryology and Genetics, Kumamoto University, 2-2-1 Honjo, Kumamoto 860-8556, Japan
*Author for correspondence (nsuzuki@doc.medic.mie-u.ac.jp)

Received 29 November 2011; Accepted 23 May 2012

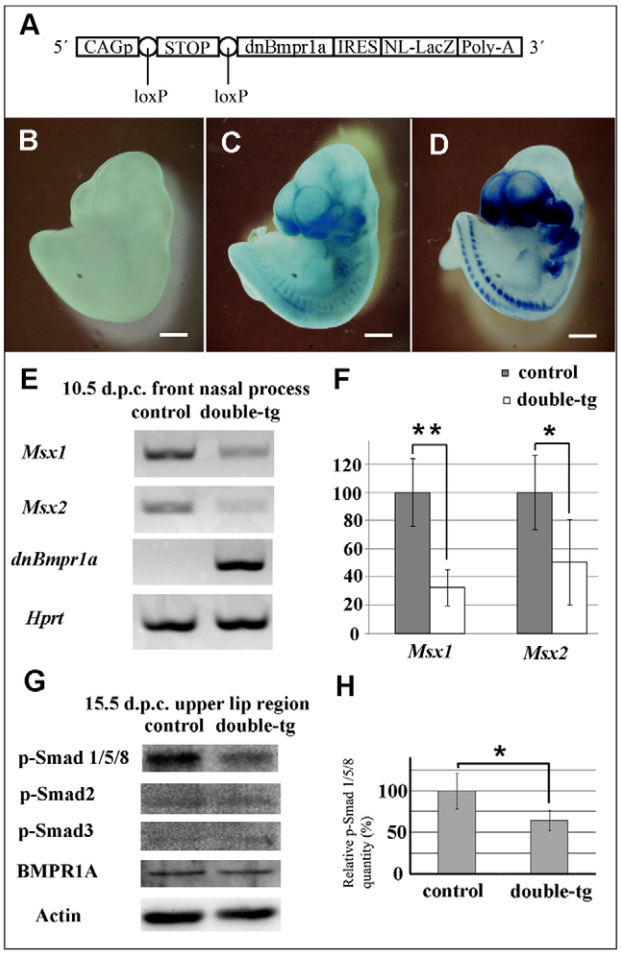

Fig. 1. Scheme of the construct expressing *dnBmpr1a* and changes in the downstream effector pathways of Bmpr1a-mediated signaling in the nasal processes of the double-tg embryos. (A) Construct *pCAG-XstopX-dnBmpr1a-IRES-NLLacZ-polyA* used for generating *Tg(CAG-flox-dnBmpr1a-NLLacZ)1Nobs* mice. (B-D) Whole-mount views of *LacZ*-stained control (B), double-tg (C) and *Tg(CAG-cat-lacZ)11Miya*$^{tg/+}$*;Tg(Mpz-cre)94Imeg*$^{tg/+}$ (D) embryos at 10.5 d.p.c. (E) RT-PCR analysis of *Msx 1*, *Msx 2* and *dnBmpr1A* expression in the nasal processes of 10.5 d.p.c. control (n=4) and double-tg (n=4) embryos. (F) Relative *Msx 1* and *Msx 2* expression levels. (G) Western blot analysis of phosphorylated Smad (p-Smad)1/5/8, p-Smad2, p-Smad3, and Bmpr1a in the upper jaws of 15.5 d.p.c. control (n=3) and double-tg (n=5) embryos. (H) Relative p-Smad1/5/8 expression levels. Error bars indicate mean ± s.e.m. *P<0.05, **P<0.01. Scale bars: 1.0 mm.

Analysis of dnBmpr1a expression by *LacZ* staining (Fig. 1B,C) confirmed that the expression pattern of dnBmpr1a was identical to that of *LacZ* in *Tg(CAG-cat-lacZ)11Miya*$^{tg/+}$*;Tg(Mpz-cre)94Imeg*$^{tg/+}$ mice (Fig. 1D). We then investigated the putative changes in the downstream effector pathways by using reverse transcriptase-polymerase chain reaction (RT-PCR) and western blot analysis of the developing nasal region at 10.5 days post coitum (d.p.c.) and 15.5 d.p.c., respectively. In the double-tg embryos, expression levels of *Msx1* and *Msx2* were significantly reduced to 32.7% (P=0.0026) and 50.6% (P=0.048) of control levels, respectively (Fig. 1E,F), and the expression of phosphorylated Smad1, Smad5 and Smad8 proteins significantly decreased to 64.5% (P=0.03) of control levels (Fig. 1G,H). However, levels of phosphorylated Smad2, phosphorylated Smad3 and Bmpr1a proteins in the nasal processes of the double-tg embryos were normal (Fig. 1G), indicating that expression of dnBmpr1a in the double-tg embryos had no effect on TGF-β pathways and endogenous Bmpr1a expression level.

Perinatal death and facial defects in the double-tg mice

At 3 weeks after birth, the ratio of double-tg was 17.9% (n=21/117). Double-tg did not show embryonic lethality but perinatal death (supplementary material Table S1). Among the newborns, 41.9% were double-tg (n=18/43). Double-tg newborns without cleft palate were indistinguishable from control newborns in appearance (Fig. 2A,B,D,E). Among the double-tg newborns, 83.3% (n=15/18) had midline fusion defects, cleft face (Fig. 2C,F) and cleft palate (Fig. 2G,H). These defects affected suckling but not breathing. The double-tg mice without cleft survived and had a characteristic short face (Fig. 2I-L). To quantify the facial morphology, we measured facial length (FL) and the distance between the eyes (DE) at 3 weeks. The FL and DE of double-tg were significantly shorter (0.87-fold; P<0.001; Fig. 2M) and greater (1.1-fold; P=0.024; Fig. 2N), respectively, than that of the controls.

Dependency of frontonasal mesenchymal cell survival on Bmpr1a-mediated signaling

At 9.5 d.p.c., which marks the end of cranial NC cell migration (Jiang et al., 2002), the double-tg embryos were histomorphologically indistinguishable from the controls (Fig. 3A,B). Furthermore, the expression pattern of *Tfap2a*, one of the marker genes of NC cells, of double-tg mice was indistinguishable from that of the controls (Fig. 3C,D). These results suggest that in our mutants NC cell migration was not affected by the reduction in Bmpr1a-mediated signaling.

At 10.5 d.p.c., the nasal processes of the double-tg mice were apparently smaller than those of the controls (Fig. 3E,F). Calculation of cell density of the frontonasal mesenchyme revealed that the cell density of the mutant embryos at 9.5 d.p.c. [(2.09±0.22)´10^4 cells/mm^2; n=3] was the same as that of the controls [(1.86±0.19)´10^4 cells/mm^2; n=3], but that the cell density of the mutant embryos at 10.5 d.p.c. was significantly lower than that of the controls (0.79-fold; P=0.002; Fig. 3G), suggesting that a decrease in proliferation and/or an increase in apoptosis occurred in the frontonasal mesenchymal cells between 9.5 and 10.5 d.p.c. Therefore, 10.5 d.p.c. nasal processes were assessed for apoptosis and proliferation. Terminal deoxynucleotidyl transferase dUTP nick end labeling (TUNEL) and P53 double staining assay of frontonasal mesenchyme showed 0% of TUNEL single-positive cells, 2.46% of TUNEL/P53 double-positive cells and 0.80% of P53 single-positive cells in the control, and 0% of TUNEL single-positive cells, 18.24% of TUNEL/P53 double-positive cells and 4.21% of P53 single-positive cells in double-tg mice (Fig. 3H-J). No TUNEL single-positive cells were detected in either double-tg or control frontonasal mesenchyme and there was a 7.4-fold enhancement in the ratio of the double-positive cells in double-tg frontonasal mesenchyme. These results indicated that the p53 apoptotic pathway was activated by a reduction in Bmpr1a-mediated signaling in double-tg frontonasal mesenchyme. RT-PCR revealed that the

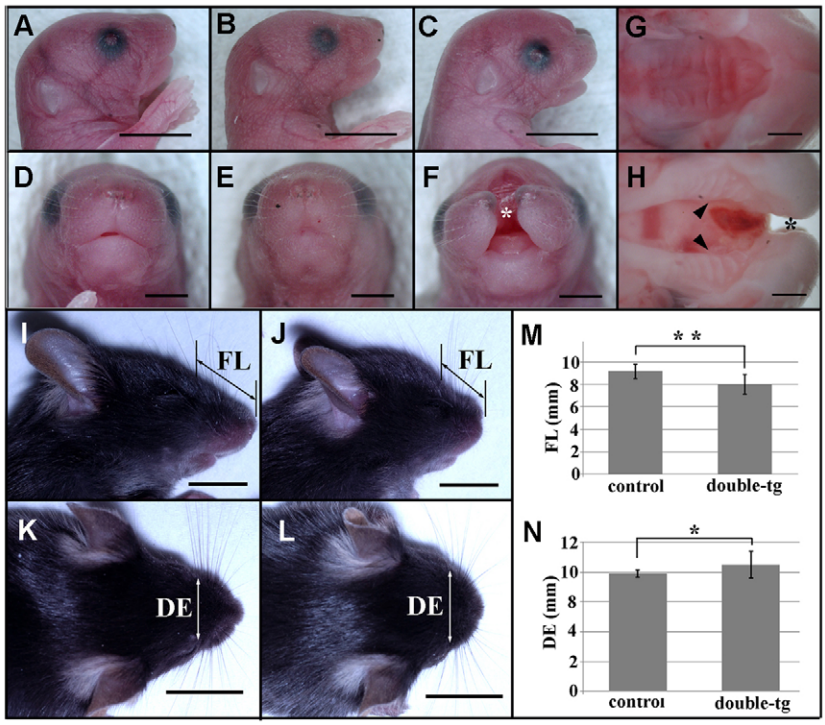

Fig. 2. Facial abnormalities of double-tg mice at later stages of development. (A-F) Lateral (A-C) and frontal (D-F) views of the control (A,D) and double-tg mice (B,C,E,F) without cleft face (B,E) and with cleft face (C,F) at birth. (G,H) Whole-mount view of a normal closed palate (G) and view of cleft palate (arrowheads) in double-tg mice (H) with facial midline cleft indicated by asterisks (F,H). (I-L) Lateral (I,J) and superior (K,L) views of control (I,K) and double-tg mice (J,L) at 3 weeks after birth. Facial length and distance between the eyes were measured and designated as FL and DE, respectively, as indicated. (M) FLs of control (n=16) and double-tg (n=11) mice. (N) DEs of control (n=16) and double-tg (n=11) mice. Error bars indicate mean ± s.e.m. *P<0.05, **P<0.001. Scale bars: 5.0 mm (A-C), 2.5 mm (D-F), 1.0 mm (G,H) and 1.0 cm (I-L).

levels of the anti-apoptotic *Bcl-XL* and the apoptosis-related *c-Myc* gene transcripts in the double-tg nasal processes were significantly reduced to 33.7% (P=0.018) and 49.2% (P=0.006) of the control levels, respectively (Fig. 3K,L). Proliferating cell nuclear antigen (PCNA) immunostaining assay showed no change in proliferation (Fig. 3M-O). At 11.5 d.p.c., when medial nasal processes normally fused in the midline (Fig. 3P), 77.8% of the double-tg embryos (n=7/9) had an abnormally unfused nasal process (Fig. 3Q). Furthermore, at both 13.5 d.p.c. and 15.5 d.p.c., after the completion of upper lip formation, 75% of double-tg embryos exhibited facial cleft (13.5 d.p.c., n=3/4; 15.5 d.p.c., n=6/8), which was consistent with the incidence of both unfused nasal processes at 11.5 d.p.c. and cleft face at birth. These observations strongly suggest that a decrement in BMP signaling induces an unusual P53-mediated apoptosis without affecting cell proliferation in the frontonasal mesenchyme around 10.5 d.p.c. and that the apoptosis eventually results in the facial cleft.

Dependency of frontal bone primordial mesenchymal cell survival on Bmpr1a-mediated signaling

Micro-computer tomographic (micro-CT) scanning at 3 weeks clearly showed calvarial ossification defects between the frontal bones of double-tg mice (n=5/5; Fig. 4A-D). No obvious defects were detected in the other parts of the double-tg skulls. Analysis of newborn skulls using Alizarin Red and Alcian Blue staining (skeletal staining) revealed a reduction in the size of the frontal bones of double-tg mice in the presence (n=3) and absence (n=1) of cleft face and cleft palate (Fig. 4E-J). The double-tg mice with cleft face and cleft palate exhibited more severe defects in craniofacial bone formation (e.g. nasal bones dysplasia and septal cartilage separation) (Fig. 4G,J). The other craniofacial bones and cartilage of the double-tg mice were indistinguishable from those of the controls. We hypothesized that the etiology of calvarial foramina is similar to that of facial dysmorphism in double-tg mice.

PCNA immunostaining and the TUNEL assay revealed an unchanged proliferation ratio and higher apoptotic ratio (2.7-fold; P=0.048), respectively, in the developing frontal bone primordial mesenchymal cells of double-tg embryos at 10.5 d.p.c. (Fig. 4K-N,Q,R). Furthermore, apoptotic p53-positive cells were detected only in the frontal bone primordia of double-tg embryos (Fig. 4O,P,S). At 12.5 d.p.c., we observed a marked reduction in the number of frontal bone primordial cells but no changes in apoptotic or proliferating cell ratios (Fig. 4T,U and data not shown). At 15.5 d.p.c., hematoxylin-eosin (HE) and skeletal staining revealed that the frontal bone primordial cells of the double-tg embryos formed the frontal bone matrix normally and differentiated into the frontal bones, but their sizes were smaller than those of the controls (Fig. 4V-Y). These observations suggest that a decrement in BMP signaling in the developing frontal bone primordial mesenchyme contributed to unusual apoptosis, which resulted in cell expansion failure around 10.5 d.p.c. This then caused a reduction in both the frontal bone primordial cell number at 12.5 d.p.c. and the frontal bone size after 15.5 d.p.c. Thus, in our model, etiology of the calvarial foramina appears to be similar to that of facial dysmorphism.

Heart septum defects and pigmentary abnormality

Because patients with juvenile polyposis syndrome and chromosome 10q23 deletion syndrome exhibit heart defects (Delnatte et al., 2006; Menko et al., 2008; Zhou et al., 2001), we assessed heart morphology in double-tg at birth by micro-CT and histomorphological analyses. Three of the six mutant mice with facial cleft (50%) exhibited a defect in the ventricular septum of the heart (supplementary material Fig. S1A-D and Movies 1, 2).

Furthermore, 28.6% of the surviving double-tg mice without cleft face or cleft palate (*n*=6/21) exhibited a pigmentary abnormality, a belly spot (supplementary material Fig. S1E).

DISCUSSION

The facial abnormalities in our double-tg mice mimic the hypertelorism and flat nasal bridge observed in patients with juvenile polyposis syndrome and chromosome 10q23 deletion syndrome. Furthermore, these patients and our double-tg mice both suffer from similar heart septal defects (Delnatte et al., 2006; Jacoby et al., 1997; Menko et al., 2008; Zhou et al., 2001). Thus, facial abnormalities and heart septal defects in human patients might be partly caused by the knockdown of BMPR1A-mediated signaling in NC-derived cells.

Compared with our double-tg mice, two previous mutant mice lacking *Bmpr1a* in NC cells exhibited more severe heart septal defects (Nomura-Kitabayashi et al., 2009; Stottmann et al., 2004) that correlated with the level of Bmpr1a-mediated signaling. However, their facial development was normal. Bmp2, Bmp4 and Bmp7 ligands bind to Bmpr1a-Bmpr1b and Bmpr2 serine/threonine kinase receptor complexes and transmit signals via common downstream proteins Smad1, Smad5 and Smad8 (R-Smads). Two

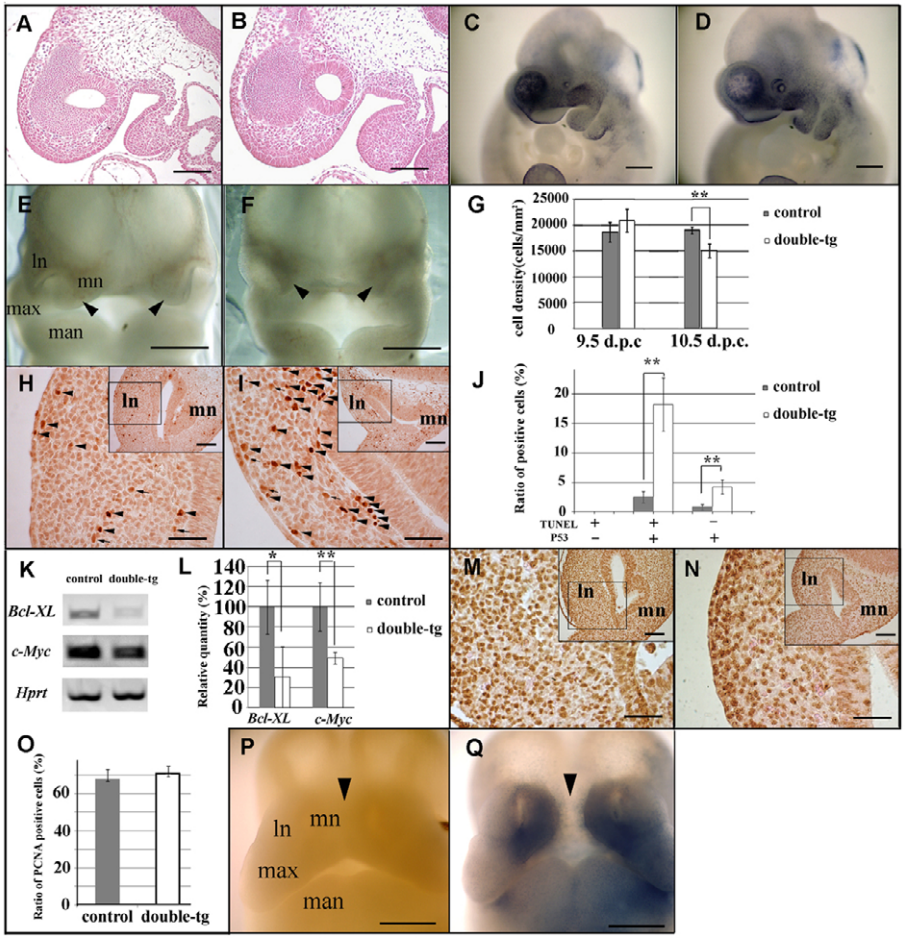

Fig. 3. Histomorphogenesis of frontonasal processes and mesenchymal apoptosis and proliferation in double-tg embryos at 9.5 and 10.5 d.p.c. (A,B) HE-stained sagittal section views of 9.5 d.p.c. control (A) and double-tg (B) embryos. (C,D) Whole mount in situ hybridization of 9.5 d.p.c. control (C) and double-tg (D) embryos. using a probe for *Tfap2a*. (E,F) Whole-mount frontal views of 10.5 d.p.c. control (E) and double-tg embryos (F). The arrowheads indicate the right and left frontonasal processes. (G) Frontonasal mesenchymal cell densities of control (*n*=4) and double-tg (*n*=4) embryos at 9.5 and 10.5 d.p.c. (H,I) Transverse sections of the nasal processes of 10.5 d.p.c. control (H) and double-tg (I) embryos stained for TUNEL reaction (black) and with anti-p53 antibody (orange); magnification of boxed areas are shown in each inset. The arrowheads and arrows in H and I indicate the TUNEL and anti-P53 immunostaining double-positive cells and anti-P53 immunostaining single-positive cells, respectively. (J) Ratio between TUNEL single-positive cells and frontonasal mesenchymal cells, ratio between TUNEL/P53 double-positive cells and frontonasal mesenchymal cells, and ratio between P53 single-positive cells and frontonasal mesenchymal cells in control (*n*=3) and the double-tg (*n*=3) embryos. (K) RT-PCR analysis of *Bcl-XL* and *c-Myc* expression in the nasal processes of 10.5 d.p.c. control (*n*=4) and double-tg (*n*=4) embryos. (L) Relative *Bcl-XL* and *c-Myc* expression levels. (M,N) Transverse sections of the nasal processes of 10.5 d.p.c. control (M) and double-tg (N) embryos stained with anti-PCNA antibody (brown) and counterstained with Kernechtrot; magnification of boxed areas are shown in each inset. (O) Ratio between PCNA-positive cells and frontonasal mesenchymal cells in control (*n*=4) and double-tg (*n*=4) embryos. (P,Q) Whole-mount frontal views of 11.5 d.p.c. *LacZ*-stained control (P) and double-tg (Q) embryos. Normally fused (*n*=2/9; data not shown) and abnormally unfused (*n*=7/9; P) nasal processes of double-tg embryos. The arrowheads in P and Q indicate the midlines of embryo faces. Max, maxillary process; man, mandibular process; ln, lateral nasal process; mn, medial nasal process. Error bars indicate mean ± s.e.m. **P*<0.05, ***P*<0.01. Scale bars: 100 μm (A,B), 200 μm (C,D), 300 μm (E,F), 50 μm (H,I,M,N), 100 μm (inset in H,I,M,N) and 500 μm (P,Q).

of any activated R-Smad proteins form a heterotrimer with a common partner, Smad4. The trimer translocates to the nucleus and regulates the transcription of target genes (Miyazawa et al., 2002). Panchision and co-workers showed that the expression levels of *Bmpr1b* in the developing heart mesenchyme of wild-type animals were much lower than those in the developing nasal mesenchyme (Panchision et al., 2001). In conditional knockout animals, the free BMPs generated by an ablation of Bmpr1a-Bmpr2 receptor complexes can bind the Bmpr1b-Bmpr2 complexes instead and transmit compensatory signals to R-Smads-Smad4 in facial development but not in heart development. In our double-tg, no free BMPs were generated because BMPs could form stable but inactive ternary complexes with dnBmpr1a-Bmpr2 receptor complexes, resulting in a failure to transmit sufficient signals for both face and heart development.

The *c-Myc* gene, a member of the helix-loop-helix family of transcription factors, is one of apoptotic regulators (Pelengaris and Khan, 2003). Both downregulation and upregulation of *c-Myc* expression are associated with an activation of apoptosis (Amendola et al., 2009; Askew et al., 1993). In our double-tg embryos, an activation of apoptosis of the frontonasal mesenchymal cells is associated with *c-Myc* downregulation. Our results showed that an optimal Bmpr1a-mediated signal was involved in maintenance of *c-Myc* expression levels in nasal process developing.

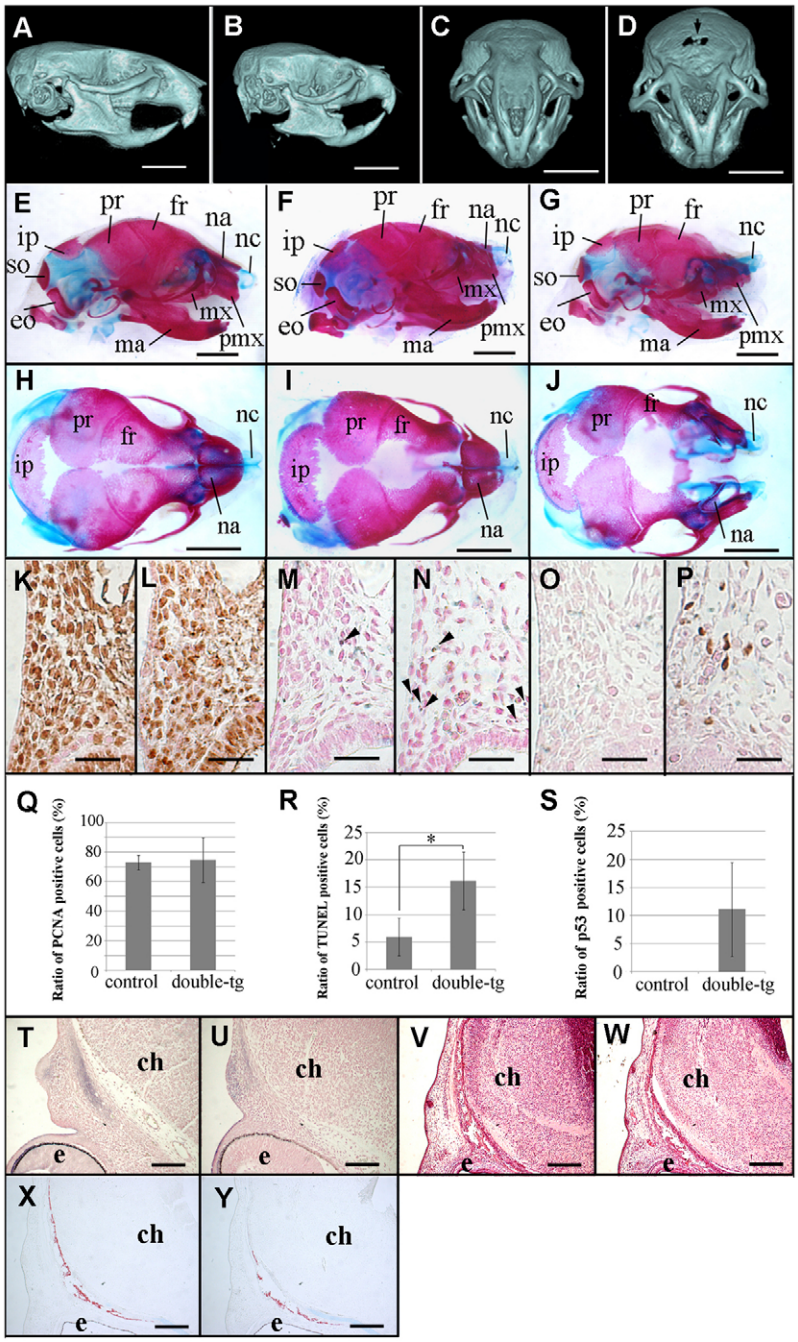

Fig. 4. Analysis of skulls and frontal bone primordia of double-tg mice. (A-D) Lateral (A,B) and frontal (C,D) CT images of the skulls of control (A,C) and double-tg (B,D) mice at 3 weeks after birth. The arrowhead in D indicates calvarial foramina. (E-J) Lateral (E-G) and superior (H-J) views of Alizarin Red- (bone) and Alcian Blue-stained (cartilage) skulls of control (E,H) and double-tg without cleft face (F,I) and with cleft face (G,J) at birth. (K,L) Transverse sections of the frontal primordium of 10.5 d.p.c. control (K) and double-tg (L) embryos stained with anti-PCNA antibody (brown) and counterstained with Kernechtrot (red). (M,N) Transverse sections of the frontal primordium of 10.5 d.p.c. control (M) and double-tg (N) embryos stained for TUNEL reaction (brown) and counterstained with Kernechtrot. (O,P) Transverse sections of the frontal primordium of 10.5 d.p.c. control (O) and double-tg (P) embryos stained with anti-P53 antibody (brown) and counterstained with Kernechtrot. P53-positive cells were not detectable in the controls (n=3). (Q) Ratio between PCNA-positive cells and frontal primordial mesenchymal cells in control (n=3) and double-tg (n=3) embryos. (R) Ratio between TUNEL reaction-positive cells and frontal primordial mesenchymal cells in control (n=3) and double-tg (n=3) embryos at 10.5 d.p.c. (S) Ratio between p53-positive cells and frontal primordial mesenchymal cells in control (n=3) and double-tg (n=3) embryos. The error bars indicate mean ± s.e.m. *P<0.05. (T,U) Transverse sections of the frontal primordium of 12.5 d.p.c. control (T) and double-tg (U) embryos stained for alkaline phosphatase (blue) and counterstained with Kernechtrot. (V,W) HE-stained transverse sections of the frontal primordium of control (V) and double-tg (W) embryos at 15.5 d.p.c. (X,Y) Alizarin Red- and Alcian Blue-stained transverse sections of the frontal primordium of control (X) and double-tg (Y) embryos at 15.5 d.p.c. ch, cerebral hemisphere; e, eye; eo, exoccipital; fr, frontal; ip, interparietal; ma, mandible; mx, maxilla; na, nasal; nc, nasal cartilage; pmx, premaxilla; pr, parietal; so, supraoccipital. Scale bars: 2.0 mm (A-F), 1.0 cm (G-J), 25 μm (K-P), 100 μm (T,U) and 200 μm (V-Y).

The NC cell-derived mesenchyme is the source for populating the frontal bone primordium in mice (Jiang et al., 2002). *Bmp2*, *Bmp4*, *Bmp7* and their receptors *Bmpr1a* and *Bmpr1b* are expressed in primordial tissues (Dewulf et al., 1995; Kim et al., 1998; Zouvelou et al., 2009). Mutations in *Msx1* and/or *Msx2* transcription factors, which are downstream in the BMP signaling pathway, result in frontal ossification defects (Han et al., 2007). These results imply that downregulation of BMP signaling via Bmpr1a in NC cells can lead to frontal bone malformation. However, early embryonic lethality of the previous *Bmpr1a* mutant mice prevented the testing of this hypothesis (Mishina et al., 1995; Nomura-Kitabayashi et al., 2009; Stottmann et al., 2004). Because our double-tg mice overcome embryonic lethality and displayed ossification defects in frontal bones, we clearly demonstrated, for the first time, a significant role of Bmpr1a-mediated signaling in normal frontal bone development.

Thus, we have developed a new useful model system for addressing the pathological mechanism of diseases caused by the downregulation of Bmpr1a-mediated signaling.

TRANSLATIONAL IMPACT

Clinical issue

Mutations in the gene encoding bone morphogenetic protein receptor type 1A (BMPR1A) are associated with facial dysmorphism and heart defects, the main clinical features of juvenile polyposis syndrome and chromosome 10q23 deletion syndrome. BMPR1A is broadly expressed and its ligands (BMP2, BMP4 and BMP7) are expressed in specific nasal regions during development. Mouse models have been used as a means to better understand the role of BMPR1A in craniofacial development. Of three previously generated conditional BMPR1A knockout mouse lines, two died in the late embryonic stage and the other did not display recombination in the mesenchymal cells of the nasal processes. In this paper, the authors developed a new mouse model that overcomes embryonic lethality, and demonstrate that features in individuals with juvenile polyposis or chromosome 10q23 deletion syndromes might be caused in part by the knockdown of BMPR1A-mediated signaling in neural crest (NC)-derived cells.

Results

The authors generated a BMPR1A knockdown mouse by conditionally expressing a dominant-negative (dn) form of BMPR1A in NC-derived cells. 100% of the conditional mutant mice had wide-open anterior fontanelles, and 80% died of cleft face and cleft palate soon after birth. The 20% that survived developed short faces, hypertelorism and calvarial foramina. 50% of mice with facial cleft at birth also showed abnormal heart morphology. Analysis of the NC-derived craniofacial mesenchyme of mutant embryos revealed a normal growth rate but an incomplete expansion of mesenchymal cells. At the molecular level, it was found that knockdown of BMPR1A-mediated signaling triggered accumulation of p53, downregulation of Bcl-XL and c-Myc, and extensive apoptosis.

Implications and future directions

These findings provide genetic evidence that optimal BMRP1A-mediated signaling is essential for NC-derived mesenchymal cell survival in normal nasal and frontal bone development. This work indicates that inhibition of BMPR1A-mediated signaling in NC-derived cells leads to facial dysmorphism and heart defects in mice that are similar to those seen in humans with juvenile polyposis syndrome and chromosome 10q23 deletion syndrome. By crossing the floxed-dnBMRP1A transgenic mice developed here with other Cre strains, it will be possible to probe the role of BMRP1A in other cell types. For example, crossing them to a colon-specific Cre mouse or a brain-specific Cre mouse will enable studies of colorectal polyposis and mental retardations, respectively, which are additional features of juvenile polyposis syndrome and chromosome 10q23 deletion syndrome.

METHODS

Mutant mice

We inserted the 0.6 kb dominant-negative mouse *Bmpr1a* cDNA (ΔmTFR11) (Suzuki et al., 1994), 0.5 kb internal ribosomal entry site and 3.5 kb *LacZ* gene containing the nuclear localization signal into the *Pme*I site of *pCAG-XstopX-polyA* (Saito et al., 2005). Founders were made by pronuclear injection into zygotes obtained by crossing *Pcp2*$^{tm1(cre)Nobs/+}$ males (129X1/SVJ*C57BL/6J) (Saito et al., 2005) and C57BL/6J females and selected by monitoring the *LacZ* expression in retina cells (data not shown). Mice heterozygous for the transgene were backcrossed to C57BL/6J for at least ten generations. All the animals were cared for in accordance with the ethical guidelines established by the Institutional Animal Care and Use Committee at Mie University.

Mutant allele genotyping

The genotypes were determined by PCR analysis. The primers for *LacZ* were as follows: *LacZ* forward, 5′-CTACACCAACCTGACCTATC-3′ and *LacZ* reverse, 5′-CGCTCATCGATAATTTCACC-3′. The primers for *Cre* were: Cre forward, 5′-GTCGATGCAACGAGTGATGA-3′ and Cre reverse, 5′-CAGCGTTTTCGTTCTGCCAA-3′. The PCR conditions were 94°C for 1 minute; 30 cycles of 94°C for 1 minute, 60°C for 1 minute, and 72°C for 1 minute; and 72°C for 5 minutes.

Statistical analysis

Data were analysed using Student's *t*-test to compare two groups. The results are presented as mean ± s.e.m.

Western blot analysis

Total protein was extracted as described previously (Tsumura et al., 2006). Rabbit antibody against phosphorylated Smad1/5/8 (Cell Signaling Technology, Beverly, MA), goat antibody against phosphorylated Smad2/3 (Santa Cruz Biotechnology), goat anti-Bmpr1a antibody (Santa Cruz Biotechnology) and rabbit anti-actin antibody (Santa Cruz Biotechnology) were used at 1:1000, 1:200, 1:200 and 1:1000 dilution, respectively. Secondary goat anti-rabbit IgG (Santa Cruz Biotechnology) and donkey anti-goat IgG (Santa Cruz Biotechnology) antibodies were both used at a dilution of 1:2000. Blotted proteins were visualized as described previously (Tsumura et al., 2006). Expression levels of proteins were normalized to that of β-actin.

RT-PCR analysis

Total RNA was extracted using Trizol reagent (Invitrogen, Carlsbad, CA). cDNA was synthesized from 1 μg of total RNA by using the reverse transcription system (Promega, Madison, WI). The primer sets were as follows: *Msx1*, 5′-ATGACTTCTTTGCCACTCGG-3′ and 5′-GTCAGGTGGTACATGCTGTA-3′; *Msx2*, 5′-ATGGCTTCTCCGACTAAAGG-3′ and 5′-GTCCATCTGGTCTTCCTTAG-3′; *dnBmpr1a*, 5′-CTGCTAACCATGTTCATGCC-3′ and 5′-GCTGCAAATACTGGTTGCAC-3′; *Bax*, 5′-ACAGATCATGAAGACAGGGG-3′ and 5′-CAAAGTAGAAGAGGGCAACC-3′; Bcl-XL, 5′-TGGTCGACTTTCTCTCCTAC-3′ and 5′-TGAGTGGACGGTCAGTGTCT-3′; c-Myc, 5′-CGCGCCCAGTGAGGATATC-3′ and 5′-CCACATAC-

AGTCCTGGATGAT-3′; and Hprt, 5′-CGTGATTAGCG-ATGATGAAC-3′ and 5′-GGCTTTGTATTTGGCTTTTC-3′.

Each experiment was performed using cDNA from the frontonasal processes of the control and double-tg mice at 10.5 d.p.c. (n=4 each). The PCR conditions were 94°C for 1 minute; 35 cycles of 94°C for 1 minute, 60°C for 1 minute, and 72°C for 1 minute; and 72°C for 5 minutes. Expression levels were normalized to that of *Hprt*.

Histological and TUNEL analysis

Histological analysis was performed as previously described (Hogan et al., 1994). For cell density analysis, we counted cells in 30,000 μm^2 area of the nasal processes in a HE-stained section of each embryo (three samples for each genotype). Primers for the 1.3-kb *Tfap2a* cDNA were: AP2 forward, 5′-ATGCTTTGGAAACTGACGGA-3′ and AP2 reverse, 5′-TTTGTCACTGCTTTTGGCGC-3′. The TUNEL assay was performed using an in situ apoptosis detection kit (Takara, Shiga, Japan). Peroxidase-conjugated anti-PCNA antibody (Dako Cytomation, Glostrup, Denmark) and rabbit anti-p53 antibody (Santa Cruz Biotechnology) were used at 1:2 and 1:1000 dilutions, respectively. Secondary goat anti-rabbit IgG antibody (Santa Cruz Biotechnology) was used at 1:2000 dilution. Signals of TUNEL, P53 and PCNA were visualized with HistoMark Black (KPL, Gaithersburg, MD), HistoMark Orange (KPL) and di-amino-benzidine (Dojindo, Kumamoto, Japan), respectively. For the statistical analysis, we counted TUNEL-, PCNA- and p53-positive cells among Kernechtrot-positive cells in the nasal processes in a section of each embryo (three or four samples for each genotype).

Micro-CT analysis

Three-dimensional images of the skulls and hearts were obtained by CT analysis using the R_mCT system (Rigaku, Tokyo, Japan). For heart analysis, mice were injected with 0.2 ml Omnipaque 350 (Daiichi-sankyo, Tokyo, Japan) via the intraorbital vein under anesthesia, and then sacrificed. The lamp voltage and current were 90 kV and 100 mA, respectively. The scanning times were 17 seconds and 2 minutes for skulls and hearts, respectively. Volume rendering and measurements were performed using the software i-View (Morita, Kyoto, Japan).

ACKNOWLEDGEMENTS

We thank Naoto Ueno (National Institute for Basic Biology) for the dominant-negative mouse *Bmpr1a* cDNA (ΔmTFR11). We also thank Drs Hidetoshi Yamazaki (Mie University), Kyoko Imanaka-Yoshida (Mie University), and Yuji Nakajima (Osaka City University) for helpful discussions.

COMPETING INTERESTS

The authors declare that they do not have any competing or financial interests.

AUTHOR CONTRIBUTIONS

H.S.: data collection and analysis, and manuscript preparation. K.Y.: *Tg(Mpz-cre)94Imeg*$^{tg/+}$ mouse preparation. N.S.: data analysis, manuscript preparation and study design. All authors edited the manuscript prior to submission.

FUNDING

This work was supported in part by Grant-in-Aid for Scientific Research, and by the National Cancer Center Research and Development Fund (23-A-2).

SUPPLEMENTARY MATERIAL

Supplementary material for this article is available at
http://dmm.biologists.org/lookup/suppl/doi:10.1242/dmm.009274/-/DC1

REFERENCES

Amendola, D., De Salvo, M., Marchese, R., Verga Falzacappa, C., Stigliano, A., Carico, E., Brunetti, E., Moscarini, M. and Bucci, B. (2009). Myc down-regulation affects cyclin D1/cdk4 activity and induces apoptosis *via* Smac/Diablo pathway in an astrocytoma cell line. *Cell Prolif.* **42**, 94-109.

Askew, D. S., Ihle, J. N. and Cleveland, J. L. (1993). Activation of apoptosis associated with enforced myc expression in myeloid progenitor cells is dominant to the suppression of apoptosis by interleukin-3 or erythropoietin. *Blood* **82**, 2079-2087.

Aubin, J., Davy, A. and Soriano, P. (2004). In vivo convergence of BMP and MAPK signaling pathways: impact of differential Smad1 phosphorylation on development and homeostasis. *Genes Dev.* **18**, 1482-1494.

Beverdam, A., Brouwer, A., Reijnen, M., Korving, J. and Meijlink, F. (2001). Severe nasal clefting and abnormal embryonic apoptosis in Alx3/Alx4 double mutant mice. *Development* **128**, 3975-3986.

Chai, Y. and Maxson, R. E., Jr (2006). Recent advances in craniofacial morphogenesis. *Dev. Dyn.* **235**, 2353-2375.

Chen, D., Zhao, M. and Mundy, G. R. (2004). Bone morphogenetic proteins. *Growth Factors* **22**, 223-241.

Danesh, S. M., Villasenor, A., Chong, D., Soukup, C. and Cleaver, O. (2009). BMP and BMP receptor expression during murine organogenesis. *Gene Expr. Patterns* **9**, 255-265.

Delnatte, C., Sanlaville, D., Mougenot, J. F., Vermeesch, J. R., Houdayer, C., Blois, M. C., Genevieve, D., Goulet, O., Fryns, J. P., Jaubert, F. et al. (2006). Contiguous gene deletion within chromosome arm 10q is associated with juvenile polyposis of infancy, reflecting cooperation between the BMPR1A and PTEN tumor-suppressor genes. *Am. J. Hum. Genet.* **78**, 1066-1074.

Dewulf, N. W., Verschueren, K., Lonnoy, O., Morén, A., Grimsby, S., Spiegle, K. V., Miyazono, K. and Huylebroeck, D. (1995). Distinct spatial and temporal expression patterns of two type I receptor for bone morphogenetic protein during mouse embryogenesis. *Endocrinology* **136**, 2652-2663.

Eblaghie, M. C., Reedy, M., Oliver, T., Mishina, Y. and Hogan, B. L. (2006). Evidence that autocrine signaling through BMPRIA regulates the proliferation, survival and morphogenetic behavior of distal lung epithelial cells. *Dev. Biol.* **291**, 67-82.

Furuta, Y. and Hogan, B. L. (1998). BMP4 is essential for lens induction in the mouse embryo. *Genes Dev.* **12**, 3764-3775.

Han, J., Ishii, M., Bringas, P., Jr, Maas, R. L., Maxson, R. E., Jr and Chai, Y. (2007). Concerted action of Msx1 and Msx2 in regulating cranial neural crest cell differentiation during frontal bone development. *Mech. Dev.* **124**, 729-745.

Hogan, B. L., Constantin, F. and Lacy, E. (1994). Manipulating the mouse embryo: a laboratory manual, Second ed. New York: Cold Spring Harbor Press.

Hu, D. and Marcucio, R. S. (2009). Unique organization of the frontonasal ectodermal zone in birds and mammals. *Dev. Biol.* **325**, 200-210.

Jacoby, R. F., Schlack, S., Sekhon, G. and Laxova, R. (1997). Del (10) (q22.3q24.1) associated with juvenile polyposis. *Am. J. Med. Genet.* **70**, 361-364.

Jiang, X., Iseki, S., Maxson, R. E., Sucov, H. M. and Morriss-Kay, G. M. (2002). Tissue origins and interactions in the mammalian skull vault. *Dev. Biol.* **241**, 106-116.

Kim, H. J., Rice, D. P., Kettunen, P. J. and Thesleff, I. (1998). FGF-, BMP- and Shh-mediated signaling pathways in the regulation of cranial suture morphogenesis and calvarial bone development. *Development* **125**, 1241-1251.

Kishigami, S. and Mishina, Y. (2005). BMP signaling and early embryonic patterning. *Cytokine Growth Factor Rev.* **16**, 265-278.

Liu, W., Sun, X., Braut, A., Mishina, Y., Behringer, R. R., Mina, M. and Martin, J. F. (2005). Distinct functions for Bmp signaling in lip and palate fusion in mice. *Development* **132**, 1453-1461.

Maéno, M., Ong, R. C., Suzuki, A., Ueno, N. and Kung, H. F. (1994). A truncated bone morphogenetic protein 4 receptor alters the fate of ventral mesoderm to dorsal mesoderm: roles of animal pole tissue in the development of ventral mesoderm. *Proc. Natl. Acad. Sci. USA* **91**, 10260-10264.

Massagué, J. (2000). How cells read TGF-β signals. *Nat. Rev. Mol. Cell Biol.* **1**, 169-178.

Menko, F. H., Kneepkens, C. M., de Leeuw, N., Peeters, E. A., Van Maldergem, L., Kamsteeg, E. J., Davidson, R., Rozendaal, L., Lasham, C. A., Peeters-Scholte, C. M. et al. (2008). Variable phenotypes associated with 10q23 microdeletions involving the PTEN and BMPR1A genes. *Clin. Genet.* **74**, 145-154.

Minkoff, R. (1980). Regional variation of cell proliferation within the facial processes of the chick embryo: a study of the role of 'merging' during development. *J. Embryol. Exp. Morphol.* **57**, 37-49.

Mishina, Y., Suzuki, A., Ueno, N. and Behringer, R. R. (1995). Bmpr encodes a type I bone morphogenetic protein receptor that is essential for gastrulation during mouse embryogenesis. *Genes Dev.* **9**, 3027-3037.

Miyazawa, K., Shinozaki, M., Hara, T., Furuya, T. and Miyazono, K. (2002). Two major Smad pathways in TGF-β superfamily signaling. *Genes Cells* **7**, 1191-1204.

Nomura-Kitabayashi, A., Phoon, C. K., Kishigami, S., Rosenthal, J., Yamauchi, Y., Abe, K., Yamamura, K., Samtani, R., Lo, C. W. and Mishina, Y. (2009). Outflow tract cushions perform a critical valve-like function in the early embryonic heart requiring BMPRIA-mediated signaling in cardiac neural crest. *Am. J. Physiol. Heart Circ. Physiol.* **297**, H1617-H1628.

Panchision, D. M., Pickel, J. M., Studer, L., Lee, S. H., Turner, P. A., Hazel, T. G. and McKay, R. D. (2001). Sequential actions of BMP receptors control neural precursor cell production and fate. *Genes Dev.* **15**, 2094-2110.

Pelengaris, S. and Khan, M. (2003). The many faces of c-Myc. *Arch. Biochem. Biophys.* **416**, 129-136.

Saito, H., Tsumura, H., Otake, S., Nishida, A., Furukawa, T. and Suzuki, N. (2005). L7/Pcp-2-specific expression of Cre recombinase using knock-in approach. *Biochem. Biophys. Res. Commun.* **331**, 1216-1221.

Stottmann, R. W., Choi, M., Mishina, Y., Meyers, E. N. and Klingensmith, J. (2004). BMP receptor IA is required in mammalian neural crest cells for development of the cardiac outflow tract and ventricular myocardium. *Development* **131**, 2205-2218.

Suzuki, A., Thies, R. S., Yamaji, N., Song, J. J., Wozney, J. M., Murakami, K. and Ueno, N. (1994). A truncated bone morphogenetic protein receptor affects dorsal-ventral patterning in the early Xenopus embryo. *Proc. Natl. Acad. Sci. USA* **91**, 10255-10259.

Tsumura, H., Yoshida, Y., Saito, H., Imanaka-Yoshida. K. and Suzuki, N. (2006). Cooperation of oncogenic K-ras and p53 deficiency in pleomorphic rhabdomyosarcoma development in adult mice. *Oncogene*, **25**, 7673-7679.

Yamauchi, Y., Abe, K., Mantani, A., Hitoshi, Y., Suzuki, M., Osuzu, F., Kuratani, S. and Yamamura, K. (1999). A novel transgenic technique that allows specific marking of the neural crest cell lineage in mice. *Dev. Biol.* **212**, 191-203.

Zhou, X. P., Woodfold-Richens, K., Lehtonen, R., Kurose, K., Aldred, M., Hampel, H., Launonen, V., Virta, S., Pilarski, R., Salovaara, R. et al. (2001). Germline mutations in BMPR1A/ALK3 cause a subset of cases of juvenile polyposis syndrome and of Cowden and Bannayan-Riley-Ruvalcaba syndromes. *Am. J. Hum. Genet.* **69**, 704-711.

Zouvelou, V., Luder, H. U., Mitsiadis, T. A. and Graf, D. (2009). Deletion of BMP7 affects the development of bone, teeth, and other ectodermal appendages of the orofacial complex. *J. Exp. Zool. B Mol. Dev. Evol.* **312B**, 361-374.